PRECLINICAL AND CLINICAL IMAGING – Rapid Communication

Magnetic Resonance in Medicine 69:1115–1121 (2013)

Diffusion Kurtosis Imaging to Detect Amyloidosis in an APP/PS1 Mouse Model for Alzheimer's Disease

Greetje Vanhoutte,[1] Sandra Pereson,[2,3] Rafael Delgado y Palacios,[1] Pieter-Jan Guns,[1,4] Bob Asselbergh,[2] Jelle Veraart,[5] Jan Sijbers,[5] Marleen Verhoye,[1] Christine Van Broeckhoven,[2,3] and Annemie Van der Linden[1]*

Purpose: Amyloid deposition in the brain is considered an initial event in the progression of Alzheimer's disease. We hypothesized that the presence of amyloid plaques in the brain of APP/presenilin 1 mice leads to higher diffusion kurtosis measures due to increased microstructural complexity. As such, our purpose was to provide an in vivo proof of principle for detection of amyloidosis by diffusion kurtosis imaging (DKI).

Methods: $APP_{KM670/671NL}$/presenilin 1 $_{L166P}$ mice ($n=5$) and wild-type littermates ($n=5$) underwent DKI at the age of 16 months. Averaged diffusion and diffusion kurtosis parameters were obtained for multiple regions (hippocampus–cortex–thalamus–cerebellum). After DKI, mice were sacrificed for amyloid staining.

Results: Histograms of the frequency distribution of the DKI parameters tended to shift to higher values. After normalization of absolute values to the cerebellum, a nearly plaque-free region, mean, radial, and axial diffusion kurtosis were significantly higher in APP/presenilin 1 mice as compared to wild-type in the cortex and thalamus, regions demonstrating substantial amyloid staining.

Conclusion: The current study, although small-scale, suggests increased DKI metrics, in the absence of alterations in diffusion tensor imaging metrics in the cortex and thalamus of APP/presenilin 1 mice with established amyloidosis. These results warrant further investigations on the potential of DKI as a sensitive marker for Alzheimer's disease. **Magn Reson Med 69:1115–1121, 2013.** © **2013 Wiley Periodicals, Inc.**

Key words: diffusion kurtosis imaging; mouse model; Alzheimer's disease

The complex progression of Alzheimer's disease (AD) involves interaction of different pathological cascades, including accumulation of amyloid-β (Aβ) and hyperphosphorylation of tau protein leading to the formation of Aβ-plaques and intracellular neurofibrillary tangles respectively. Together with associated processes such as inflammation and oxidative stress, these cascades contribute to loss of synaptic integrity and progressive neurodegeneration, eventually resulting in cognitive deficits in patients. In 2010, worldwide 36 million people suffered from dementia and the majority have AD, a striking figure that is predicted to almost quadruple by 2050 (1–3).

Despite huge investments of resources to develop and validate clinical biomarkers of AD, potential biomarkers all have their shortcomings and none is adequate enough for effective diagnosis of AD. Moreover, postmortem histopathological analysis demonstrating Aβ-plaques in the brain remains the gold standard for accurate and final diagnosis of AD.

As Aβ accumulation and the subsequent formation of Aβ-plaques starts at the early phase of the disease (4) many of the biomarker approaches are based on the early detection of Aβ-peptides and/or Aβ-plaques.

Detection of $A\beta_{40}$-, $A\beta_{42}$-peptides and their respective ratio in the cerebral spinal fluid has been proposed for clinical diagnosis of AD. Indeed, it has been shown that the cerebral spinal fluid concentration of $A\beta_{42}$—the main constituent of Aβ-plaques—decreases upon development of brain plaques. The down side of this approach is the invasive nature of the cerebral spinal fluid collection procedure (5).

In addition, various neuro-imaging tools have been proposed for noninvasive monitoring of Aβ-load. Various radio-tracers have been developed and claim to selectively bind to Aβ-plaques (^{11}C-PiB-PET (6,7), ^{18}F-florbetapir (Amyvid®)-PET (8,9), ^{18}F-florbetaben (BAY 949172-PET) (10)). Despite these recent advances in PET-imaging of AD, most radioligands are not ideal for quantification due to low signal-to-noise ratio, nonspecific binding or unfavorable kinetics, and radiation burden.

[1]Department of Biomedical Sciences, Bio-Imaging Lab, University of Antwerp, Antwerp, Belgium.

[2]Department of Molecular Genetics, VIB, Antwerp, Belgium.

[3]Laboratory of Neurogenetics, Institute Born-Bunge, University of Antwerp, Antwerp, Belgium.

[4]Expert Group Antwerp Molecular Imaging (EGAMI), University of Antwerp, Antwerp, Belgium.

[5]Department of Physics, IMinds-Vision Lab, University of Antwerp, Antwerp, Belgium.

Grant sponsor: Interuniversity Attraction Poles program of the Belgian Science Policy Office, Methusalem Excellence program of the Flemish Government, Research Foundation Flanders (FWO), and Agency for Innovation by Science and Technology (IWT), Belgium; Grant sponsor: EC-FP7 project NAD; Grant number: CP-IP 212043-2; Grant sponsor: European Unionhx0027;s Seventh Framework Programme (FP7/2007-2013); Grant number: HEALTH-F2-2011-278850 (INMiND); Grant sponsor: Interuniversity Attraction Poles Programme (IUAP 7/11) initiated by the Belgian Science Policy Office.

*Corresponding to: Vanhoutte Greetje, Universiteit Antwerpen, Bio-Imaging Lab, Universiteitsplein,1, Campus Drie Eiken, Building UC, 2610 Antwerpen, Belgium. E-mail: Greetje.Vanhoutte@ua.ac.be

Received 18 October 2012; revised 21 December 2012; accepted 14 January 2013

DOI 10.1002/mrm.24680

Published online 11 March 2013 in Wiley Online Library (wileyonlinelibrary.com).

Magnetic resonance imaging (MRI) is another imaging technique which in contrast to PET relies on intrinsic tissue contrast generation. Furthermore, MRI combines high spatial resolution with superior soft tissue contrast. MRI volumetry, a gold standard measurement in dementia (11), has proven-value to detect brain atrophy, however, brain atrophy represents the final stages of AD when irreversible damage and clinical symptoms have already manifested.

So far, two strategies have been followed using MRI for amyloid detection in AD: a first approach involves the application of contrast enhancing agents that specifically bind to Aβ-plaques in mouse models (12). A second methodology is dependent on the detection of Aβ-plaque related susceptibility artifacts in both mouse models (13–15) and humans (16). Although promising, the latter approach showed no irrevocable success and is not specific enough.

In this study, we explored the use of diffusion kurtosis imaging (DKI) as a novel, noncontrast dependent tool for detection of amyloidosis in APP/presenilin 1 (PS1) transgenic mice.

DKI, as any other diffusion-weighted (DW) MRI-method, measures diffusion-driven displacements of water molecules which bounce off, interact with or cross many ultrastructural boundaries, such as cell and organelle membranes and macromolecules in and out the cell. These interactions impede the movement of the water molecules and the actual diffusion distance will be reduced as compared with that of free water. Consequently, the displacement distribution is no longer Gaussian. Considering that DKI takes into account the non-Gaussianity of diffusion in biological tissues (17), it reflects better the genuine characteristic of diffusion in the brain as compared to conventional diffusion tensor imaging (DTI) (18–20). Recent DKI-studies in rat have illustrated many advantages of DKI to reveal changes in microstructural complexity of the brain in Huntington's disease (21), in a cortical impact injury model (22), in a chronic mild stress model (23), in a stroke model (24) and experimental ischemia (25).

In the present study, we have hypothesized that the presence of extracellular Aβ-plaques adds up to the complexity of the brain on a microstructural level. Given the fact that DKI offers more information compared to conventional DTI to detect changes in microstructural complexity, DKI might be able to detect Aβ-plaque-related increased microstructural complexity.

To this end, DKI measurements were performed in old APP/PS1 mice. The APP/PS1 transgenic mouse model is a well-documented model of cerebral amyloidosis. These mice start to develop Aβ-plaques from the age of 2 months, which cover the whole cerebrum from the age of 8 months onwards. APP/PS1 mice do not display tau-pathology or global neurodegeneration, however, the robust cerebral amyloidosis in APP/PS1 mice shows similar progression to that of AD patients (26). In the current study, DKI was explored in 16-month-old APP/PS1 mice. At this age, the mice should have massive cerebral amyloidosis covering the whole cerebrum (26,27). The use of such a robust model of amyloidosis is ideal to demonstrate proof of principle for detection of Aβ-plaques by DKI.

METHODS

Animal Model for AD

APP/PS1 transgenic mice co-expressing hAPP harboring the Swedish double mutation KM670/671NL and PS1 carrying the L166P mutation were compared to wild-type (WT) littermates at the age of 16 months (per group $n = 5$) (26). All animal procedures and husbandry were performed in accordance with the European Communities Council Directive (86/609/EEC) and approved by the Committee on Animal Care and Use at the University of Antwerp.

Diffusion Kurtosis Acquisition and Analysis

DKI was conducted on a 9,4T MRI system (Bruker Biospec, Ettlingen Germany). Mice were anaesthetized using isoflurane (1.5–2%) and monitored to maintain constant physiological parameters. The DKI protocol included the acquisition of seven non-DW images and 210 DW images with the use of seven *b*-values (400, 800, 1200, 1600, 2000, 2400, and 2800 s/mm^2) and 30 non-collinear diffusion gradient directions. Images were collected with a multislice two-shot SE-EPI sequence (pulse repetition time/echo time = 7500/24 ms, $\delta = 5$ ms, $\Delta = 12$ ms, acquisition matrix = 96 × 64, zero filled to 128 × 64, spatial resolution: (150 × 200 × 500) μm^3, NEX = 4). The DKI model was voxel-wise fitted to the normalized DW images to allow a more accurate description of the Gaussian, as well as the non-Gaussian diffusion of water molecules (28). The DKI tensors were assessed using weighted least squares estimators, which quantify the apparent diffusion coefficient and the deviation from Gaussian diffusion (17,29). From the tensor information diffusion parametric maps were computed using Matlab routines (The Mathworks Inc., Natick, MA) [fractional anisotropy, axial- (AD), radial- (RD), and mean-diffusivity (MD)] as well as additional diffusion kurtosis parameters [mean- (MK), axial- (AK), and radial-kurtosis (RK)]. Regions-of-interest (ROI) were delineated in AMIRA (Mercury Computer systems, San Diego) based on grey values of b_0 images and were verified on fractional anisotropy and mean-diffusivity maps to minimize partial volume effects.

Averaged diffusion and diffusion kurtosis parameters were obtained for multiple regions (somatosensory cortex (ctx, average of five slices), hippocampus (hip, average of three slices), and thalamus (thal, average of two slices). In addition, regional values of each parameter were also expressed as a ratio to the cerebellum (cbll) (parameters are indicated with a prefix "r" e.g.: rMK). Figure 1 illustrates the ROI selection as delineated according to the Paxinos Mouse Brain Atlas (30) for the various brain tissues, covered in multiple coronal slices. DKI metrics were presented graphically both as histograms (0.01 bins) and mean absolute values as relative ratio's to the cerebellum reference region.

Amyloid Plaque Quantification

After DKI acquisition, APP/PS1 mice were sacrificed for histopathological evaluation of amyloid plaque load. Two 4-μm thick serial sections were stained with 1%

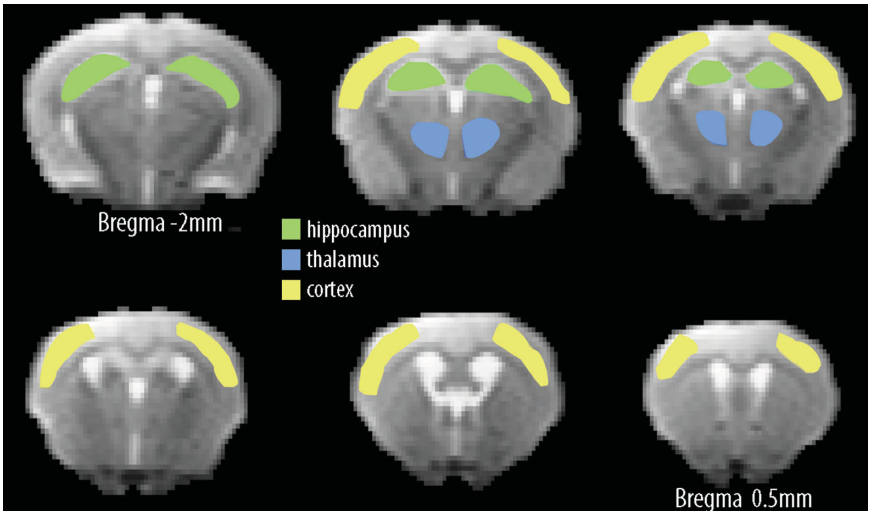

FIG. 1. Illustration of ROI delineation of the hippocampus, the thalamus and the cortex according to the Paxinos Mouse Brain Atlas overlaid on six consecutive non-DW images (500-μm thickness). Colour codes: hippocampus: green, thalamus: blue, cortex: yellow).

thioflavin S (Sigma), followed by differentiation in 70% ethanol. All sections were stained simultaneously and no antigen retrieval or counter staining was performed. Images were acquired on an Axiovert 200M fluorescent microscope (Carl Zeiss, Zaventem, Belgium), using identical excitation and camera exposure settings. Overlapping images comprising the complete brain were acquired at 10× magnification. Stitching of the images was performed with the MosaiX module from Zeiss Axiovision software, resulting in single TIF images (pixel size 1.3 μm) that were exported and further analyzed in ImageJ (31). The different brain regions were outlined according to a mouse brain atlas (30) and saved as ImageJ ROI files. A custom made ImageJ analysis script was used to measure the tissue area and the area covered by amyloid plaques in batch for all brain regions on all images. The tissue area was segmented by separating tissue ruptures and background with the imageJ "Huang" intensity thresholding method. The plaque area was detected by intensity thresholding with the "Triangle method" and "Analyze particle" command. The resulting segmented regions were checked visually afterwards. The percentage amyloid plaque load was obtained by dividing the plaque area by the tissue area in each region.

Statistics

Results are expressed as mean ± S.E.M., ($n = 5$ DKI (APP/PS1 and WT); $n = 3$ histology (APP/PS1 only). A genotype effect (APP/PS1 mice versus WT littermates) was assessed for all DKI parameters using a nonparametric Mann Whitney U test with significance level $P = 0.05$ (SPSS 16.0, SPSS Inc., Chicago)

RESULTS

Amyloid plaque load of the APP/PS1 mice was evaluated by thioflavin S staining which revealed regional differences in amyloid load (Fig. 2). The highest amyloid plaque load (expressed as percentage volume per tissue volume) was observed in the thalamus (1.77 ± 0.20) followed by the cortex (1.45 ± 0.12). The cortical value is higher than the hippocampal value (1.12 ± 0.19), whereas the cerebellum has a negligible amount of amyloid (0.08 ± 0.02). DKI parameters were assessed in specific ROIs represented in Figure 1. ROI analysis was performed for the hippocampus, the thalamus and the cortex, delineated according to the Paxinos Mouse Brain Atlas (30).

For the diffusion kurtosis parameters, no significant differences were demonstrated when comparing mean absolute values of transgenic APP/PS1 with WT mice. Although histogram representation suggested a shift of mean-kurtosis, radial-kurtosis, and axial-kurtosis in the thalamus and cortex region towards higher diffusion kurtosis values (Fig. 3). This was not the case for the hippocampus and the cerebellum, where the diffusion kurtosis distributions of the APP/PS1 and WT group overlap. When diffusion kurtosis parameters were normalized to the nearly plaque-free cerebellum reference region, rMK, rRK, and rAK of both thalamic and cortical

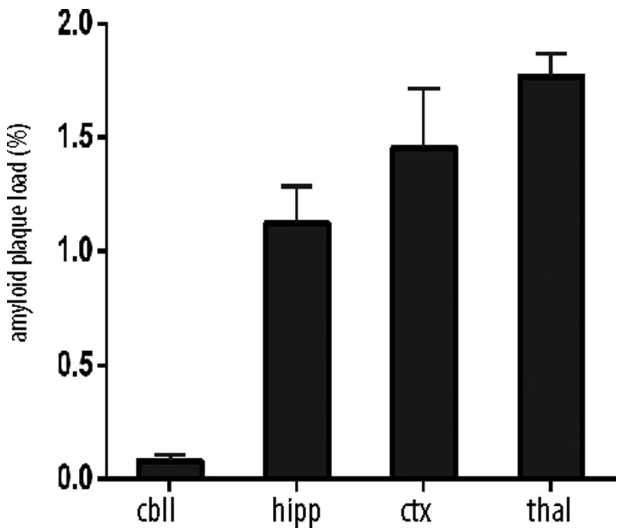

FIG. 2. Regional amyloid load of brain sections ($n = 3$) stained with thioflavin S. Plaque area versus tissue area is expressed as mean amyloid load percentage ±S.E.M. for each region (cbll = cerebellum, hipp = hippocampus, ctx = cortex, and thal = thalamus). A regional difference in the amyloid plaque load is shown.

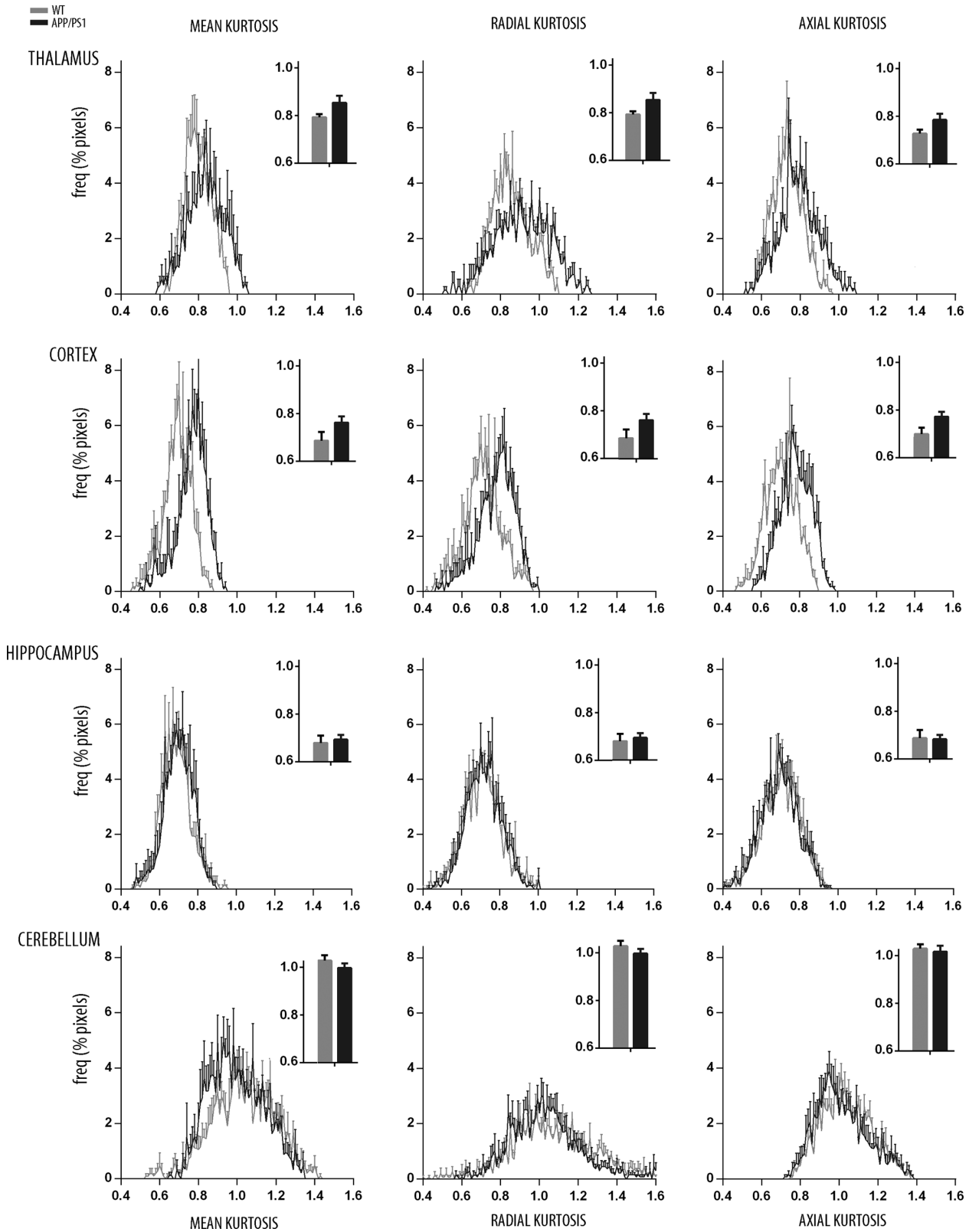

FIG. 3. Histograms show frequency distributions (percentage) of diffusion kurtosis values (bin size 0.01) per ROI for three diffusion kurtosis parameters. For the thalamus and the cortex, the histograms of the APP/PS1 are shifted to higher kurtosis values. Histograms for APP/PS1 and the WT are overlapping for the cerebellum and the hippocampus. Bar graphs display absolute DKI values. Data are presented as mean±S.E.M.; WT $n=5$; APP/PS1 $n=5$).

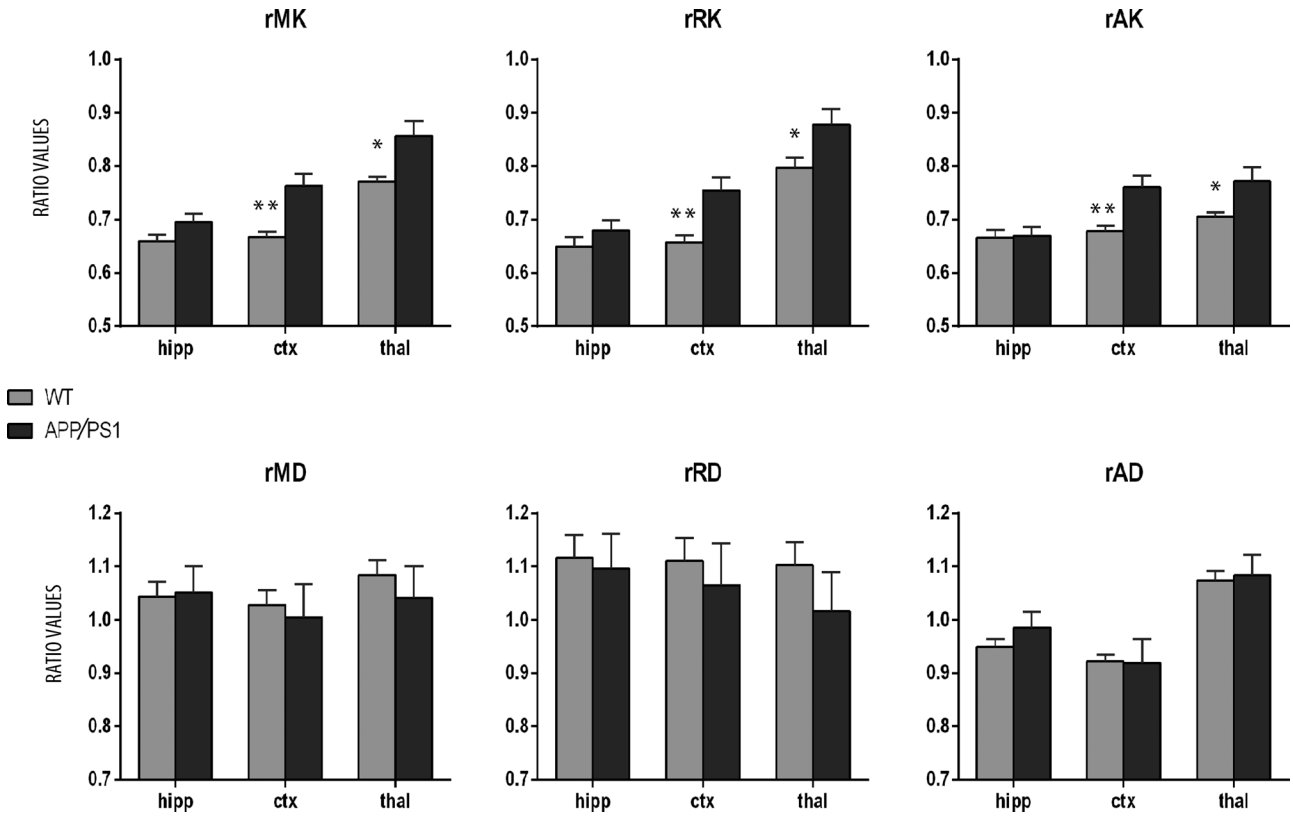

FIG. 4. Bar graphs represent diffusion kurtosis and diffusion parameters expressed as ratio to the cerebellum ('r' prefixed, MK = mean kurtosis, RK = radial kurtosis, AK = axial kurtosis, MD = mean diffusion, RD = radial diffusion, AD = axial diffusion, hipp = hippocampus, ctx = cortex, and thal = thalamus). Data are expressed as mean ± S.E.M., $n = 5$, significant group effects: $^{*}P < 0.05$ and $^{**}P < 0.01$.

regions differed significantly from the values obtained in WT mice (Fig. 4): rMK, rRK, and rAK were significantly elevated in the APP/PS1 group (cortex $P = 0.004$, $P = 0.008$, $P = 0.009$ and thalamus $P = 0.016$, $P = 0.046$, $P = 0.042$ respectively). For the diffusion parameters (mean-diffusivity, radial-diffusivity and axial-diffusivity), both expressed as mean absolute value or relative ratio's, no genotype differences were observed in any of the analyzed region.

DISCUSSION

DKI as a Measure for Aβ-Plaque-Induced Increased Microstructural Complexity

This current study reports increased DKI metrics in the cortex and thalamus of APP/PS1 mice whereas no alterations in DTI parameters were observed. These results are in line with the hypothesis that Aβ-plaques add to the microstructural complexity of the brain and with a previous observation from Falangola et al. (32) using DKI in ex vivo formalin-fixed brains of 20 month old APP/PS1 mice. Although formalin-fixed brains might be less favorable to study water diffusion in physiological circumstances, such study can target the brain anatomy at the ultrastructural level. Furthermore, since no changes could be picked up with conventional DTI parameters, our results confirm the added value of DKI compared to DTI to scrutinize pathologies affecting the microstructure in gray matter, whereas DTI has rather proven-value to study white matter changes in mouse models for AD (33,34).

Regional Differences in Plaque Load and DKI

The APP/PS1 mouse that we used in the current study provides a robust model of cerebral amyloidosis. Interestingly, the region-dependent pattern of progressive Aβ pathology in the APP/PS1 mice is similar to that described in AD patients (26). At the time point of the DKI acquisition the amyloid pathology was pronounced in the cortex, thalamus, and hippocampus whereas the cerebellum remained virtually plaque-free (Fig. 2). This distinct regional pattern of Aβ-plaques within the cerebrum allows for interpretation of the DKI data in the context of amyloid burden.

As anticipated, all DKI parameters (rMK, rRK, and rAK) were significantly increased in the cortex and thalamus, however, the hippocampus showed no increased diffusion kurtosis metrics despite the presence of a substantial amyloid load. The latter might be related to a different interaction between Aβ-plaques and neurons in the hippocampus compared to the thalamus or cortex. Indeed, it has recently been shown by histopathological evaluation that in the hippocampus of 17 months old APP/PS1 mice there was significant local neuron loss in the vicinity of Aβ-plaques (27), whereas this phenomenon was not observed in the cortex. We speculate that the local loss of neurons in the hippocampus might counterbalance the

increased diffusion kurtosis caused by Aβ-plaques. In the cortical regions Rupp et al. showed a different situation. Cortical neurons in the vicinity of Aβ-plaques appeared to be displaced, forming neuronal dense boundary around the Aβ-plaques instead of neuronal loss.

The different behavior of the DKI metrics in the hippocampus in response to amyloid plaque load demonstrates that DKI results in general should be interpreted with caution. Based on the current results DKI shows potential to detect amyloidosis, although not only the amount of amyloid influences the diffusion kurtosis but also associated processes such as neurodegeneration, neuroinflammation (21,22,35), or ageing (35) might affect DKI metrics as well.

Ratio to the Cerebellum

Although the histogram representation suggested a shift of DKI parameters to higher values in the cortex and the thalamus of APP/PS1 mice, no significant changes in absolute values were observed. This absence of statistical difference might be related to relatively high intersubject variability in combination with a low *n*-number. Interestingly, after normalization to the virtually plaque free cerebellum, DKI metrics reached significant difference in the cortex and thalamus. Similarly, the majority of the PET-amyloid imaging studies in AD (in human and animal studies) also report target-to-cerebellar retention ratios (36). Whether the normalization procedure applied in the current study might be of clinical value cannot be extrapolated from this current study with a limited sample size. Further exploration and validation of this ratio strategy in preclinical or clinical studies with larger sample size would definitely be interesting.

DKI as Early Marker for AD?

Nowadays, MRI volumetry detecting the magnitude and pattern of brain atrophy is the gold standard for late-stage AD diagnosis. However, biomarkers to identify early AD are lacking. As current treatment approaches target the prevention or the reversal of Aβ-plaque deposition in the brain (37), DKI might be an important tool for evaluating their efficacy. Our results of increased DKI parameters in transgenic mice with amyloidosis show potential for such application in the clinic. To our opinion, DKI could become part of a larger integrated diagnostic framework that allows MRI fingerprinting of AD pathology, both in early stages, disease progression and late stage.

Limitations of the Study

Although the Aβ-plaque load was significantly increased in specific brain areas (cortex and thalamus) and an increase of diffusion kurtosis parameters was observed in the same regions, other processes might be involved in diffusion kurtosis changes as well. To elucidate the exact underlying mechanism(s) a separate analysis with specific emphasis on co-registration of DKI with extensive histology data at the voxel level should be a focus of future DKI studies in AD. A longitudinal study to investigate early changes of DKI in APP/PS1 mice, as well as further unraveling the unanticipated behavior of hippocampal DKI parameters has been initiated, but is beyond the scope of the present short communication. The current study illustrates proof of concept of DKI to detect amyloidosis in APP/PS1 mice. Although it is based on a low sample size, which might be suboptimal for statistical analysis, this outcome bears potential for further exploration of DKI in the future.

CONCLUSION

In conclusion, the current study, although small-scale, suggests already increased DKI metrics, in the absence of alterations in DTI metrics in the cortex and thalamus of APP/PS1 mice with established amyloidosis. These results warrant further investigations on the potential of DKI as a sensitive marker for AD.

ACKNOWLEDGMENTS

The authors acknowledge the company KOESLER (Rottenburg, Germany) and Dr. Mathias Jucker (University of Tubingen) for providing the APPPS1 mice. The research was performed in the frame of the international consortium of Centers of Excellence in Neurodegenerative Brain Diseases (CoEN, http://www.coen.org/) supported by the Flemish Government through the VIB. S.P. received a PhD fellowship of the IWT.

REFERENCES

1. Ballard C, Gauthier S, Corbett A, et al. Alzheimer's disease. Lancet 2011;377:1019–1031.
2. Citron M. Strategies for disease modification in Alzheimer's disease. Nat Rev Neurosci 2004;5:677–685.
3. Herbert CP. Cultural aspects of dementia. Can J Neurol Sci 2001;28 (Suppl 1):S77–S82.
4. Lopresti BJ, Klunk WE, Mathis CA, et al. Simplified quantification of Pittsburgh Compound B amyloid imaging PET studies: a comparative analysis. J Nucl Med 2005;46:1959–1972.
5. Engelborghs S, Le Bastard N. The impact of cerebrospinal fluid biomarkers on the diagnosis of Alzheimer's disease. Mol Diagn Ther 2012;16:135–141.
6. Svedberg MM, Rahman O, Hall H. Preclinical studies of potential amyloid binding PET/SPECT ligands in Alzheimer's disease. Nucl Med Biol 2012;39:484–501.
7. Vlassenko AG, Benzinger TL, Morris JC. PET amyloid-beta imaging in preclinical Alzheimer's disease. Biochim Biophys Acta 2012;1822: 370–379.
8. Fleisher AS, Chen K, Liu X, et al. Using positron emission tomography and florbetapir F18 to image cortical amyloid in patients with mild cognitive impairment or dementia due to Alzheimer disease. Arch Neurol 2011;68:1404–1411.
9. Sperling RA, Johnson KA, Doraiswamy PM, et al. Amyloid deposition detected with florbetapir F 18 ((18)F-AV-45) is related to lower episodic memory performance in clinically normal older individuals. Neurobiol Aging 2013;34:822–831.
10. Schipke CG, Peters O, Heuser I, et al. Impact of beta-amyloid-specific florbetaben PET Imaging on confidence in early diagnosis of Alzheimer's disease. Dement Geriatr Cogn Disord 2012;33:416–422.
11. Li TQ, Wahlund LO. The search for neuroimaging biomarkers of Alzheimer's disease with advanced MRI techniques. Acta Radiol 2011;52:211–222.
12. Wadghiri YZ, Hoang DM, Wisniewski T, et al. In vivo magnetic resonance imaging of amyloid-beta plaques in mice. Methods Mol Biol 2012;849:435–451.
13. Teipel SJ, Kaza E, Hadlich S, et al. Automated detection of amyloid-beta-related cortical and subcortical signal changes in a transgenic model of Alzheimer's disease using high-field MRI. J Alzheimers Dis 2011;23:221–237.

14. Vanhoutte G, Dewachter I, Borghgraef P, et al. Noninvasive in vivo MRI detection of neuritic plaques associated with iron in APP[V717I] transgenic mice, a model for Alzheimer's disease. Magn Reson Med 2005;53:607–613.
15. Helpern JA, Lee SP, Falangola MF, et al. MRI assessment of neuropathology in a transgenic mouse model of Alzheimer's disease. Magn Reson Med 2004;51:794–798.
16. Sperling R, Salloway S, Brooks DJ, et al. Amyloid-related imaging abnormalities in patients with Alzheimer's disease treated with bapineuzumab: a retrospective analysis. Lancet Neurol 2012;11:241–249.
17. Jensen JH, Helpern JA, Ramani A, et al. Diffusional kurtosis imaging: the quantification of non-gaussian water diffusion by means of magnetic resonance imaging. Magn Reson Med 2005;53:1432–1440.
18. Cheung MM, Hui ES, Chan KC, et al. Does diffusion kurtosis imaging lead to better neural tissue characterization? A rodent brain maturation study. Neuroimage 2009;45:386–392.
19. Grinberg F, Farrher E, Kaffanke J, et al. Non-Gaussian diffusion in human brain tissue at high b-factors as examined by a combined diffusion kurtosis and biexponential diffusion tensor analysis. Neuroimage 2011;57:1087–1102.
20. Wang JJ, Lin WY, Lu CS, et al. Parkinson disease: diagnostic utility of diffusion kurtosis imaging. Radiology 2011;261:210–217.
21. Blockx I, De GG, Verhoye M, et al. Microstructural changes observed with DKI in a transgenic Huntington rat model: evidence for abnormal neurodevelopment. Neuroimage 2012;59:957–967.
22. Zhuo J, Xu S, Proctor JL, et al. Diffusion kurtosis as an in vivo imaging marker for reactive astrogliosis in traumatic brain injury. Neuroimage 2012;59:467–477.
23. Palacios R, Campo A, Henningsen K, et al. Magnetic resonance imaging and spectroscopy reveal differential hippocampal changes in anhedonic and resilient subtypes of the chronic mild stress rat model. Biol Psychiatry 2011;70:449–457.
24. Hui ES, Du F, Huang S, et al. Spatiotemporal dynamics of diffusional kurtosis, mean diffusivity and perfusion changes in experimental stroke. Brain Res 2012;1451:100–109.
25. Cheung JS, Wang E, Lo EH, et al. Stratification of heterogeneous diffusion MRI ischemic lesion with kurtosis imaging: evaluation of mean diffusion and kurtosis MRI mismatch in an animal model of transient focal ischemia. Stroke 2012;43:2252–2254.
26. Radde R, Bolmont T, Kaeser SA, et al. Abeta42-driven cerebral amyloidosis in transgenic mice reveals early and robust pathology. EMBO Rep 2006;7:940–946.
27. Rupp NJ, Wegenast-Braun BM, Radde R, et al. Early onset amyloid lesions lead to severe neuritic abnormalities and local, but not global neuron loss in APPPS1 transgenic mice. Neurobiol Aging 2011;32:2324–2326.
28. Veraart J, Poot DH, Van Hecke W, et al. More accurate estimation of diffusion tensor parameters using diffusion Kurtosis imaging. Magn Reson Med 2011;65:138–145.
29. Veraart J, Van Hecke W, Sijbers J. Constrained maximum likelihood estimation of the diffusion kurtosis tensor using a Rician noise model. Magn Reson Med 2011;66:678–686.
30. Paxinos G, Franklin K. The mouse brain in stereotactic coordinates, 2nd ed. Dan Diego: Academic Press; 2001.
31. Schneider CARWS, Eliceiri KW. NIH image to ImageJ:25 years of image analysis. Nat Methods 2012;9:671–675.
32. Falangola MF, Branch C, Jensen JH, et al. Assessment of brain microstructure in a transgenic mouse model of β-amyloid deposition. In Proceedings of the 15th Annual Meeting of ISMRM, Berlin, Germany, 2007. p. 310.
33. Song SK, Kim JH, Lin SJ, et al. Diffusion tensor imaging detects age-dependent white matter changes in a transgenic mouse model with amyloid deposition. Neurobiol Dis 2004;15:640–647.
34. Sun SW, Song SK, Harms MP, et al. Detection of age-dependent brain injury in a mouse model of brain amyloidosis associated with Alzheimer's disease using magnetic resonance diffusion tensor imaging. Exp Neurol 2005;191:77–85.
35. Falangola MF, Jensen JH, Babb JS, et al. Age-related non-Gaussian diffusion patterns in the prefrontal brain. J Magn Reson Imaging 2008;28:1345–1350.
36. Manook A, Yousefi BH, Willuweit A, et al. Small-animal PET imaging of amyloid-beta plaques with [11C]PiB and its multi-modal validation in an APP/PS1 mouse model of Alzheimer's disease. PLoS One 2012;7:e31310.
37. Delrieu J, Ousset PJ, Caillaud C, et al. 'Clinical trials in Alzheimer's disease': immunotherapy approaches. J Neurochem 2012;120 (Suppl 1): 186–193.